Analysis and Comparison of 24 GHz cmWave Radio Propagation in Urban and Suburban Scenarios

Rodriguez, Ignacio; Portela Lopes de Almeida, Erika; Abreu, Renato; Lauridsen, Mads; Loureiro, Alexandre; Mogensen, Preben Elgaard

Published in:
Wireless Communications and Networking Conference (WCNC), 2016 IEEE

DOI (link to publication from Publisher):
10.1109/WCNC.2016.7564893

Publication date:
2016

Document Version
Accepted author manuscript, peer reviewed version

Analysis and Comparison of 24 GHz cmWave Radio Propagation in Urban and Suburban Scenarios

Ignacio Rodriguez[1], Erika P. L. Almeida[1,2], Renato Abreu[2], Mads Lauridsen[1], Alexandre Loureiro[2], and Preben Mogensen[1]

[1]Wireless Communication Networks Section, Department of Electronic Systems, Aalborg University, Denmark.
Emails: {irl, eplda, ml, pm}@es.aau.dk

[2]Instituto de Desenvolvimento Tecnológico (INDT), Manaus/Brasília, Brazil.
Emails: {erika.almeida, renato.abreu, alexandre.loureiro}@indt.org.br

***Abstract*—This paper presents a measurement-based comparison of cm-wave propagation in urban and suburban scenarios at 24 GHz with transmitter antennas located above rooftop level. Different sets of directional measurements, exploring the full azimuth and the range from -30 to +30 degrees in elevation, were performed with horn antennas located close to street level, in order to explore the spatial characteristics of the channel in both LOS and NLOS conditions. The statistical analysis of different directional indicators shows how, at 24 GHz, outdoor propagation is quite different in the suburban scenario as compared to the urban case. Increased spatial multipath, in average 1.23 times higher, is observed in the suburban scenario, mainly due to the strong presence of vegetation. This results in reduced suburban NLOS path loss exponents (3.4) in comparison to the urban scenario (3.7), as detailed in the outdoor path loss analysis. The paper also highlights the potential of using beam combining techniques in order to improve cell-edge coverage by 17% and 37% in the urban and suburban scenarios, respectively. Outdoor-to-indoor propagation was also investigated, finding an average penetration loss of 6.5 dB for buildings composed of light construction materials. The different results and observations provided in the paper are useful for modeling and simulation of future wireless networks operating at 24 GHz in urban and suburban scenarios.**

***Keywords*—cmWave, 24 GHz, Radio Propagation, Urban, Suburban, Spatial Multipath, Path Loss, LOS, NLOS, Beam Combining Gain, Penetration Loss.**

I. Introduction

To overcome the spectrum scarcity below 6 GHz and guarantee the requirements of future wireless systems, as for example 5G cellular, the use of cm-wave (3-30 GHz) and mm-wave (30-300 GHz) frequency bands is being currently investigated by academia and industry [1]. While the mm-wave frequency bands have attracted the most of the research focus during the last years [2], the potential of cm-wave spectrum for commercial wireless access remains largely unexplored, especially for frequency bands above 20 GHz. This upper part of the cm-wave spectrum has been traditionally used for fixed point-to-point wireless links, local multipoint distribution services (LMDS), automotive radar, and satellite and military communications, but there are still more than 2 GHz of spectrum available, that could be used for cellular access [3].

Before enabling the use of this spectrum for a particular application, it is essential to explore and characterize the radio propagation in order to enable researchers to fully understand the potential and limitations of deploying future networks operating at these frequencies in different scenarios and conditions. There are still few studies in the literature reporting measurements and propagation analysis for the frequency range 20-30 GHz with focus on point-to-multipoint access. Most of the works focused on propagation for 26 and 28 GHz LMDS urban and rural scenarios where the receiver antenna is typically placed above rooftop level, in a much higher position than in typical cellular scenarios [4, 5]. More recently, a series of wideband measurements performed in New York at 28 GHz have already shown the viability of using cm-wave frequencies in outdoor urban deployment scenarios for covering areas up to approximately 200 m, even in non-line-of-sight (NLOS) conditions [6]. Based on the previous measurements, different spatial channel characteristics were explored in [7], finding a multipath-rich environment that could be exploited favorably by using smart receivers with beam combining capabilities [8]. As illustrated in [9], by using non-coherent beam combining, an increased coverage of approximately 230-270 m could be achieved in urban scenarios. Not only spatial characteristics were analyzed for the 28 GHz New York scenario, different path loss studied were published and have been summarized in [10], where path loss exponents of 1.9 in line-of-sight (LOS) and 3.5-3.8 in NLOS are reported for directionally obtained power samples.

This paper complements the previous work by presenting a measurement-based comparison of propagation in urban and suburban scenarios at 24 GHz. There are two main novelties in the paper. One is the inclusion of the suburban scenario, which has not attracted much attention yet as potential candidate for cm-wave deployments. The other is the frequency considered which, even being "close" to 28 GHz, remains unexplored for this type of scenarios and could perform slightly different. The comparison is presented in terms of different directional multipath statistical parameters such as angle spread, number of peak components, angle-of-arrival or lobe angle spread. The study is completed with an outdoor and outdoor-to-indoor path loss evaluation, together with an estimation of the potential gains in case of using non-coherent beam combining.

The rest of the paper is organized as follows: Section II describes the different aspects related to the measurement campaign. Sections III and IV, presents the directional analysis and the path loss investigation, respectively. Finally, Section V concludes the paper.

II. Measurement Campaign

A. Measurement Setup

In order to perform the measurements, the directional setup shown in Fig. 1 was used. It consisted of 22 dBi gain pyramidal horn antennas with a half-power beamwidth (HPBW) of 25 degrees at both the transmitter (TX) and receiver (RX) sides. As depicted in the overview of the overall measurement system in Fig. 2, a 24 GHz continuous-wave (CW) was generated in the R&S SMF100A signal generator, amplified, and delivered to the TX antenna for transmission, resulting in an approximated effective isotropic radiated power (EIRP) of +34 dBm. The TX antenna was mounted on a 2 m high tripod and fixed to a particular orientation and downtilt angle in order to cover different specific areas. At the RX side, the antenna was mounted at 1.75 m height, on a pedestal with semi-automated rotation capabilities (automated in azimuth, manual-operated in elevation). The received signal was pre-amplified using a low-noise amplifier and recorded with the R&S FSW67 spectrum analyzer. The resolution bandwidth was set to 10 kHz, resulting in a sensitivity of -120 dBm. By using this setup, and assuming a minimum signal-to-noise ratio (SNR) of 10 dB, the maximum measurable path loss was estimated to be approximately 170 dB. Only vertical polarization was considered.

Fig. 1. Directional measurement setup with TX antenna on a tripod with fixed orientation, and RX antenna mounted on a semi-automated rotating pedestal.

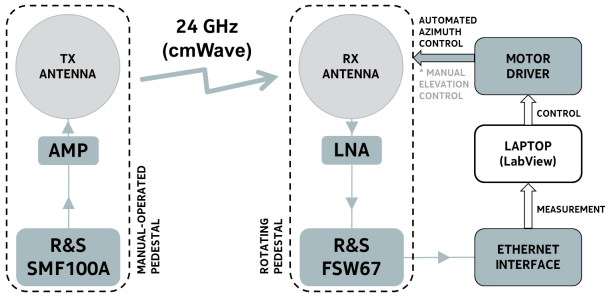

Fig. 2. Overview of the measurement system.

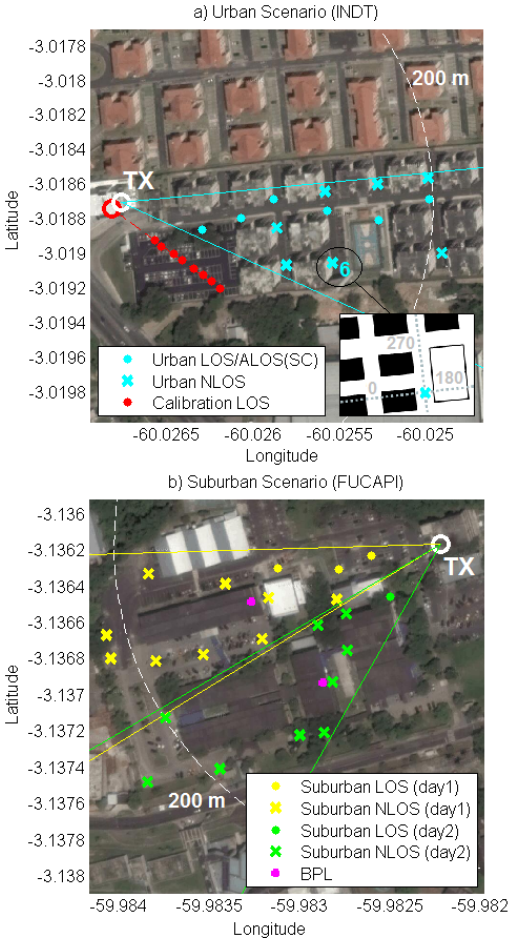

Fig. 3. Aerial view of the urban and suburban scenarios.

B. Measurement Scenarios

The measurement campaign was performed in Manaus, Amazonas, Brazil, in April, 2015. As mentioned in the previous section, the study focuses on comparing the propagation in urban and suburban scenarios, so two different locations were considered:

1) Urban scenario (INDT): residential area that resembles a 3GPP Manhattan grid urban scenario, with regular blocks of buildings (approximately 15 m tall) and street canyons (Fig. 3.a). A single TX orientation was considered aiming to illuminate a main street canyon (SC). Measurements were performed in the aforementioned canyon in line-of-sight (LOS) and almost-LOS (ALOS) conditions (obstructed TX-RX link, but still fairly good signal level due to typical urban canyon "waveguiding" effects), as well as in the perpendicular streets in clear non-line-of-sight (NLOS) conditions.
2) Suburban scenario (FUCAPI): university campus area conformed by large scattered buildings, open spaces and strong presence of vegetation in comparison with the urban scenario (Fig. 3.b). In this case, two TX orientations were considered in separate days, in order to perform measurements in a larger area of interest with different LOS and NLOS distances. No ALOS conditions were detected at any selected measurement point in this scenario.

TABLE I
SUMMARY OF THE NUMBER AND TYPE OF LOCATIONS AND MAXIMUM DISTANCES MEASURED IN EACH OF THE DIFFERENT SCENARIOS

	URBAN (cyan)	**SUBURBAN** (yellow)	(green)
# LOS/ALOS POINTS	1/5	3/0	1/0
# NLOS POINTS	7	9	9
MAX. TX-RX DISTANCE	210 m	225 m	250 m
# BPL SAMPLES (magenta)	-	1	1

In both scenarios, the TX antenna was deployed on the flat rooftop of 4-storey building at approximately 15 m above ground level with a downtilt angle of 5 degrees. Fig. 3 displays an aerial view of the two scenarios and the selected measurement positions inside the HPBW areas illuminated by the TX. Table I summarizes the number of measurement points as well as the different propagation conditions and the maximum distance range for each of the TX configurations in the two scenarios. The color code indicated in the table facilitates a better understanding of Fig.3. As it can be seen, not only outdoor propagation was explored, a couple of building penetration loss (BPL) measurements were also conducted at the suburban scenario, in order to get an estimation on outdoor-to-indoor penetration loss as well.

C. Measurement Procedures and Calibration

In order to explore the directional characteristics of the channel, at each selected measurement position a total of 280 (40x7) directional samples were recorded. Each of these values corresponds to a different angle-of-arrival (AoA) in the range from 0 to 360 degrees in steps of 9 degrees in azimuth and from -30 to +30 degrees in steps of 10 degrees in elevation. The RX antenna was manually set to the correspondent elevation, while the full azimuth rotation and measurement process was automatized using dedicated LabView software. Both the azimuth and elevation angular resolutions, smaller than half of the HPBW, ensure a correct sampling and peak power detection. Each of the directional samples is calculated as the average value of 10 sub-samples recorded by the spectrum analyzer at each particular azimuth and elevation with a sampling rate of 2 Hz.

In order to calibrate the measurement system, an open space LOS calibration was performed. 8 measurements were collected, in the parking lot, along the red discontinuous line shown in Fig. 3.a. This calibration route covered distances in-between 37 and 86 m, and the TX and RX antennas were aligned in boresight direction. By using these LOS samples, path loss (PL) was computed as indicated in (1),

$$PL = EIRP - P_{RX} + G_{RX} + G_{RF} \quad \text{[dB]} \qquad (1)$$

where $EIRP$ is the effective isotropic radiated power in dBm, P_{RX} is the received power recorded by the spectrum analyzer in dBm, G_{RX} is the RX antenna gain in dBi, and G_{RF} is a constant value of 5 dB accounting for all the extra RF combined gain introduced at RX side by the cable, connectors and the low-noise pre-amplifier.

The resultant LOS calibration path loss samples are shown in Fig. 4. As it can be seen, they present a good match with the free space path loss (FSPL) reference. This calibration was further validated by considering also the measurements from the different LOS points obtained later in the measurement campaign at the urban and suburban scenarios. By considering the entire set of samples, a small standard deviation of 1.4 dB is observed with respect to the FSPL reference.

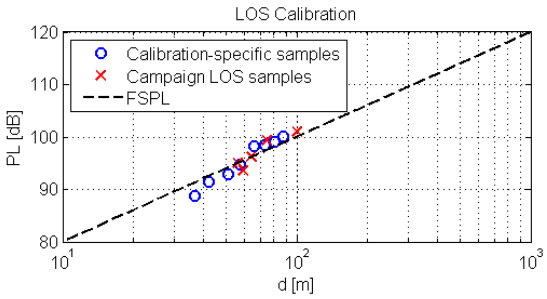

Fig. 4. LOS path loss calibration samples and comparison with FSPL.

III. DIRECTIONAL ANALYSIS

Based on the power samples obtained directionally at each of the considered measurement points, an extensive probabilistic analysis was performed. Several statistical parameters were evaluated with the aim of comparing the different spatial/directional multipath characteristics in the urban and suburban scenarios.

The first parameter explored is angle spread (AS), which is a measure of how multipath is concentrated in a single azimuthal direction, in respect to a mean angle of arrival or departure [11]. The mathematical definition is given in (2),

$$AS = \sqrt{1 - \frac{|F_1|^2}{F_0^2}} \quad \text{[-]} \qquad F_n = \int_0^{2\pi} p_{rx}(\theta)\, e^{jn\theta} d\theta \qquad (2)$$

where θ denotes the azimuth angle in radians, F_n is the n-th Fourier coefficient of the angular distribution of the directional multipath power $p_{rx}(\theta)$. The angle spread is normalized by the total amount of local average received power. An angle spread of 1 means that propagation does not favor any specific direction, while an angle spread of 0 indicates an azimuthal concentration.

Fig. 5.a shows the cumulative distribution function (CDF) of the angle spread for the two considered scenarios. In the suburban case, AS is closer to 1, which denotes no clear bias in the angular distribution of received power. In general, energy arrives simultaneously from many different directions as compared to the urban case, in which the street canyon guiding effects have a clear impact in condensing the energy around a single main angle of arrival.

The remaining parameters considered in this section are lobe statistics, which account for the different directions at which the signal arrives to the receiver antenna and the spread of energy around those main directions. In order to find the lobes, peak detection was performed over the different sets of directional power data. Lobes are identified by applying a threshold of 20 dB from the strongest received component, considering always minimum SNR of 10 dB above the noise floor, as illustrated in Fig. 6. This particular example, shows a

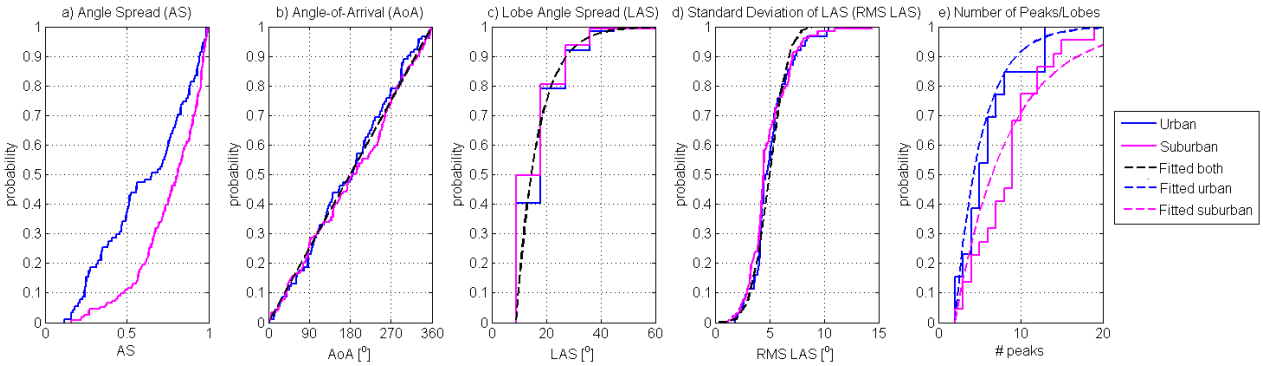

Fig. 5. Statistical analysis of different directional channel indicators.

total of 6 peaks/lobes detected in the NLOS position 6 in the urban scenario (see Fig. 3.a for azimuth angular reference).

Angle-of-arrival (AoA, $\bar{\theta}$) is defined as the mean direction of arrival of a lobe [2] and computed as (3),

$$\bar{\theta} = \frac{\sum_k p(\theta_k)\theta_k}{\sum_k p(\theta_k)} \quad [^o] \tag{3}$$

where θ_k is the k-th pointing angle (in degrees) within a lobe, and $p(\theta_k)$ represents the directional power (in linear scale).

The AoA CDFs shown in Fig. 5.b consider data from all the azimuths and elevations at all the different measurement points considered and, as it can be seen, they are very similar for the urban and suburban scenarios. They both match well to a uniform distribution between 0 and 360 degrees, which means that, in both scenarios, the signal can arrive at the RX from any particular random direction. This is quite a different situation compared to the one experienced in low-frequency bands (i.e. 2 GHz), where the AoA was mainly dominated by the geometrical TX-RX azimuth in both LOS and NLOS [12], which seems not to be the case anymore (except in very clear LOS). This difference can be explained by the different propagation mechanisms. While in low-frequency bands outdoor propagation is mainly driven by diffraction, at higher frequencies, reflection and scattering become dominant and increase the randomness of the AoA [13]. Similar observations were reported in [7] based on 28 GHz measurements in a dense urban scenario.

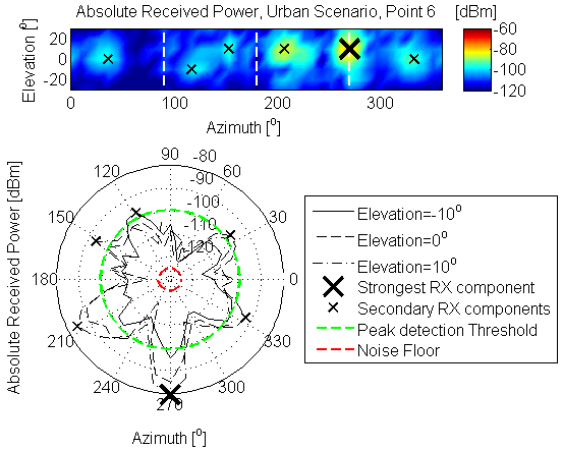

Fig. 6. Example of peak/lobe detection. The threshold is set to 20 dB from the strongest received component with a minimum SNR of 10 dB.

Lobe angle spread (LAS) represents the angle span of a lobe, above the selected threshold of 20 dB from the peak power. The standard deviation of lobe angle spread (RMS LAS), defined in (4), accounts for the angle span of the lobe in which most power is received [2].

$$RMS\ LAS = \sqrt{\overline{\theta^2} - \left(\bar{\theta}\right)^2} \quad [^o] \qquad \overline{\theta^2} = \frac{\sum_k p(\theta_k)\theta_k^2}{\sum_k p(\theta_k)} \tag{4}$$

Figs. 5.c and Fig. 5.d show, respectively, the CDFs of LAS and RMS LAS. Similar distributions were found for the urban and suburban scenarios. LAS can be well modeled as an exponential distribution with a rate parameter (λ) of 8 degrees, over a constant value of 9. Note that the LAS steps of 9 degrees are due to the azimuth angular resolution from the measurement data, in practice, LAS could present values starting from zero, but they would still fit to an exponential distribution with slightly higher rate parameter. This is not a limiting factor for the study since the main objective was to compare propagation in the urban and the suburban scenarios with respect to different metrics, and according to this, in terms of LAS both scenarios are equal. As it could be expected after finding a similar LAS, both the urban and suburban scenarios are similar in terms of RMS LAS, which can be modeled as a normal distribution with a mean of 5 degrees and a standard deviation of 1.8 degrees.

Further insight on the spatial multipath propagation in the scenarios is obtained by analyzing the different number of peaks/lobes at a particular RX location, which is representative of the number of potential strong spatial components between TX and RX. Fig. 5.e shows the CDFs of the number of peak/lobes detected by considering all the measured positions in the different scenarios. As it can be seen, the number of peaks detected at the explored positions in the suburban scenario (median of 9 peaks) is higher than in the urban scenario (median of 5 peaks). This correlates well with the AS (Fig.5.a) results and conclusions previously presented. The main difference between the urban and suburban scenario is the strong presence of vegetation in the suburban scenario. By visual inspection of the data and the different AoA over a map, it was possible to verify that a large amount of strong components is originated in the trees (scattering) and present higher, or at least comparable, signal levels compared to other components (i.e. reflections on the buildings).

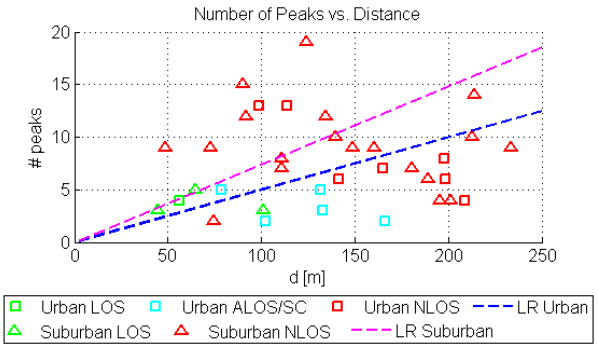

Fig. 7. Number of peaks detected vs. distance and propagation conditions.

The observed number of peak/lobes can be modeled as a constant value of 2 plus an exponential function with rate parameter of 3.5 for the urban scenario, and 6.5 (higher) for the suburban scenario.

To conclude the directional analysis, Fig.7, illustrates the correlation between the amount of spatial multipath (number of peaks), the different propagation conditions and distance. By looking at the data for the different propagation conditions, it is clear that the amount of spatial components in both scenarios is much higher in NLOS compared to LOS. The average number of peaks detected in LOS conditions in the urban and suburban scenarios is very similar, while in NLOS the number of components detected is higher in the suburban case. This can be related once again to the impact of vegetation, which contributes favorably to the overall propagation in the scenario. In average, the number of NLOS peaks is 1.23 times higher in the suburban scenario than in the urban scenario. Linear regression (LR) was applied over the data in both scenarios to compute a very simple linear model able to capture the amount of multipath at different distances. The resultant model coefficients are approximately 0.05 peaks/m for the urban scenario and 0.07 peaks/m for the suburban scenario. The number of peaks at a particular location found in the urban scenario is slightly smaller than the one reported in [6] based on 28 GHz measurements in a dense urban scenario. This could be due to the different material composition of the buildings in our Brazilian urban scenario compared to most of the construction materials used in the buildings in New York, which are reinforced and increase the reflectivity [14].

IV. Path Loss Analysis

A. Outdoor Propagation

After exploring the directional channel characteristics, the study is completed with a path loss analysis combined with different beam combining gain (BCG) estimations performed for the different scenarios. In beam combining, the power contained in various lobes is combined to obtain a higher received power level. This is one of the potential features for the future smart receivers with adaptive antenna systems able to fully exploit the rich multipath existing at cm-wave and mm-wave frequencies [2, 8]. BCG is defined in (5),

$$BCG = P_{RX,combined} - P_{RX,single} \quad \text{[dB]} \qquad (5)$$

as the power level difference between the power levels, in dBm, of the strongest (SINGLE) peak component ($P_{RX,single}$) and the (COMBINED) power resulting from the non-coherent addition in linear domain of the power from the three strongest received components ($P_{RX,combined}$) at each particular measurement position.

Table II shows the potential BCG for the different conditions and scenarios. As explained before, beam combining benefits from multipath, so the gains are larger (approximately 1.5 dB) in NLOS compared to LOS conditions. Scenario-wise, the suburban scenario allows for approximately 3 dB gain in NLOS conditions, 0.8 dB larger than the estimated gain in the urban scenario in the same conditions.

TABLE II
AVERAGE BEAM COMBINING GAIN FOR THE DIFFERENT SCENARIOS

	URBAN			SUBURBAN		
	LOS	**NLOS**	**AVG**	**LOS**	**NLOS**	**AVG**
BCG [dB]	0.8	2.2	1.6	1.6	3.0	2.8

Based on the different single and combined power samples computed, path loss (PL) was calculated by applying (1). The resultant PL samples are shown in Fig. 8 for the different conditions and scenarios. Two path loss models were used to evaluate the PL data. The first one, the alpha-beta (AB) model, is a floating reference model, with two coefficients and free fit to the data. The expression for the model is given in (6), where α accounts for the offset in dB and β for the slope of the model. Differently, the close-in (CI) model, is a reference point model, where the offset is predefined to the free-space path loss value calculated at a particular reference distance (d_0). In this case, as it can be seen from the model expression given in (7), a single coefficient n accounting for the slope needs to be calculated, since the wavelength (λ) is known at each particular frequency. Both models consider distance (d) in m.

$$PL_{AB} = \alpha + 10 \cdot \beta \cdot \log_{10}(d) \quad \text{[dB]} \qquad (6)$$

$$PL_{CI} = 20 \cdot \log_{10}\left(\frac{4\pi d_0}{\lambda}\right) + 10 \cdot n \cdot \log_{10}\left(\frac{d}{d_0}\right) \quad \text{[dB]} \qquad (7)$$

Table III contains the different coefficients for the models derived by using least-square linear regression fit over the different sets of data. A lot of discussions are ongoing in the research community about which of the models is better suited for statistical path loss modeling of cm-wave and mm-wave frequency bands [2, 10, 15]. In this case, due to the limited set of data, the CI model is more adequate [15]. Both the AB and CI models predict similar PL levels in NLOS, however, in the urban LOS scenario, the AB model underestimates the PL for the short distances, due to the few points and the LOS/ALOS/SC categorization.

The CI model with reference distance of 1 m is shown, together with the path loss samples, in Fig. 8. As it can be seen in the figure and read from the coefficients in Table III, the propagation in LOS is very close to free-space with n (path loss exponent) close to 2 in both the urban and

TABLE III
SUMMARY OF THE AB AND CI PATH LOSS MODEL COEFFICIENTS AND ROOT MEAN SQUARE ERROR (RMSE) FOR THE DIFFERENT SCENARIOS AND LOS/NLOS CONDITIONS CONSIDERING SINGLE OR COMBINED POWER SAMPLES

		SINGLE				COMBINED			
		URBAN		SUBURBAN		URBAN		SUBURBAN	
		LOS/ALOS/SC	NLOS	LOS	NLOS	LOS/ALOS/SC	NLOS	LOS	NLOS
AB	α [dB]	32.0	58.0	69.0	49.8	31.6	63.1	57.1	47.3
	β [-]	3.7	3.8	1.5	3.9	3.7	3.4	2.1	3.8
	RMSE [dB]	4.04	7.89	1.16	11.65	4.11	8.22	2.08	12.04
CI	n ($d_0 = 1$ m)	2.3	3.7	2.0	3.4	2.3	3.6	1.9	3.2
	RMSE [dB]	4.60	7.89	1.16	11.69	4.72	8.21	2.03	12.12
	n ($d_0 = 2.5$ m)	-	-	2.0	3.7	-	-	1.9	3.6
	RMSE [dB]	-	-	1.32	11.6	-	-	2.03	12.09

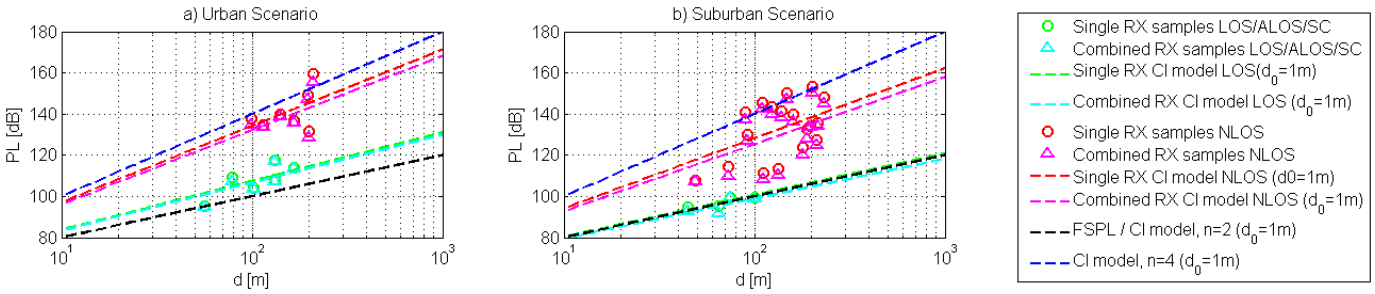

Fig. 8. Path loss samples estimated from the single and combined power and CI model with 1 m reference distance for the different scenarios.

suburban scenarios. This is true for both the single and combined power samples, as there is not so much gain by combining in LOS. On the other hand, in NLOS, the path loss exponents are slightly different in the urban and suburban scenario. By considering the single power samples, path loss exponents of 3.7 and 3.4 (lower) are observed in the urban and suburban scenarios, respectively. This results are in line with the path loss exponents find in the 28 GHz New York analysis presented in [10]. When beam combining is considered, the NLOS path loss exponents are reduced in 0.3 for the urban scenario and 0.4 for the suburban scenario.

An interesting aspect to be considered, is that the urban and suburban NLOS scenarios can be modeled by the same path loss exponents (3.7) when considering the CI model over a reference distance of 1 m in the urban scenario and 2.5 m (larger) in the suburban scenario. This observation tries to point out that, when addressing statistical linear path loss models, the fixed reference parameter could be both the distance (offset) or the propagation exponent (slope).

To conclude the outdoor path loss analysis, an estimation of the potential coverage extension achievable in the different scenarios by using beam combining is performed. This is done by evaluating the two metrics defined in [9]: distance extension exponent (DEE) and distance extension factor (DEF). DEE is defined in (8) and quantifies the potential cell range extension in terms of path loss exponent ratio between n_1 and n_2, which are the path loss exponents estimated for single strongest components and for combined power samples, respectively. DEF, defined in (9), translates the DEE into distance ratio calculated over a reference cell radius (d_1) considered in m.

$$DEE = \frac{n_1}{n_2} \quad [-] \tag{8}$$

$$DEF = {d_1}^{(DEE-1)} \quad [-] \tag{9}$$

TABLE IV
NLOS BEAM COMBINING DISTANCE EXTENSION EXPONENTS AND FACTORS FOR THE DIFFERENT SCENARIOS

	URBAN	SUBURBAN
n_1 (SINGLE)	3.7	3.4
n_2 (COMBINED)	3.6	3.2
DEE	1.02	1.06
DEF ($d_1 = 200$ m)	1.17	1.37

Table IV summarizes the different DEE and DEF calculated for the urban and suburban scenario based on the path loss exponents previously obtained. The resulting DEE applied over a reference cell radius distance (d_1) of 200 m, results into an extended coverage of 234 m in the case of the urban scenario and 274 m in the case of the suburban scenario. As a reference, in [9], an extended cell radius of 261 m is estimated by assuming 3-component non-coherent combining in a dense urban scenario (New York) at 28 GHz. The larger distance range obtained in that case can be explained with the findings from previous directional multipath analysis. The Brazilian urban scenario is a little bit less reflective than the New York scenario due to different building construction materials, so smaller beam combining gains are expected.

B. Outdoor-to-Indoor Penetration Loss

Outdoor-to-indoor propagation was investigated for the two buildings marked with magenta points on Fig. 3.b. These buildings were specifically selected because their doors were facing the TX position and, after a couple of azimuth scans, it was possible to verify that, even with the door closed, the signal propagated inside through the door. Building penetration loss (BPL) is defined in (10), as the difference between the peak power measured inside the building in the direction of the entrance with the door open ($P_{RX,open}$) or closed ($P_{RX,closed}$), both in dBm. The resulting BPL values are summarized in Table V.

TABLE V
BUILDING PENETRATION LOSS MEASURED AT THE TWO DIFFERENT BUILDINGS CONSIDERED IN THE SUBURBAN AREA

BUILDING	$P_{RX,open}$ [dBm]	$P_{RX,closed}$ [dBm]	BPL [dB]
1	-60.61	-67.71	7.10
2	-90.87	-96.86	5.98

$$BPL = P_{RX,open} - P_{RX,closed} \quad \text{[dBm]} \tag{10}$$

Penetration loss is mainly related to the type and nature of the construction materials used [14, 16], so it is also expected that buildings in the urban area present a similar attenuation since they are very much alike in composition. The average BPL calculated from the two buildings is 6.5 dB. This "low" value was expected since the buildings are composed of light materials such as walls made of thin layers of brick and concrete and clean glass single-layered windows. According to our previous studies, we can classify it as an "old building" [16] and our model for this type of constructions predicts 7.8 dB at this frequency [17], so a good match is observed.

V. CONCLUSIONS AND FUTURE WORK

This paper presented a measurement-based comparison of 24 GHz cm-wave propagation in urban and suburban scenarios when transmitter antennas are located above rooftop level. A set of directional measurements, exploring the full azimuth from 0° to 360° and elevations between -30° and 30°, was performed at different locations with standard gain horn antennas located close to street level.

The statistical analysis of different directional indicators shows how the outdoor propagation can be quite different in the suburban scenario as compared to the urban case. The main differences are observed in NLOS conditions, where the number of multipath components in the suburban scenario was found to be 1.23 times higher than in the urban scenario. This is mainly due to the presence of vegetation in the suburban scenario, which translates into strong scattered components from the trees that contribute favorably to the propagation. The potential of future smart antenna systems with beam-forming capabilities at the receiver was also evaluated, estimating an average three-component non-coherent beam combining gain of 2.2 dB and 3 dB in NLOS conditions in the urban and suburban scenarios, respectively.

The overall outdoor path loss was also analyzed and modeled by a close-in 1 m reference model. For the urban scenario, path loss exponents of 2.3 and 3.7 are found for LOS and NLOS conditions, respectively. In the suburban case, the path loss exponents are slightly smaller and equal to 2 for LOS and 3.4 for NLOS. By considering NLOS beam combining capabilities, the NLOS path loss exponents are reduced to 3.6 for the urban scenario and 3.2 for the suburban scenario. Altogether, by assuming a reference cell size of 200 m, coverage could be extended up to 234 m in the urban case, and 274 m in the suburban case. Outdoor-to-indoor propagation was also investigated for two different buildings made of light construction materials, finding an average penetration loss of 6.5 dB, which is in line with previous studies.

As future work, a more specific analysis of the impact of the vegetation observed in the suburban scenario will be considered, as well as a ray-tracing analysis that will help to model the individual contributions from each of the different propagation mechanisms in each of the scenarios.

ACKNOWLEDGMENT

This study was partially supported by Fundação Centro de Análise, Pesquisa e Inovação Tecnológica (FUCAPI). The authors would like to express their gratitude to Carlla Martins, Lilian Ramalho, Edson Silva, and Edmilson Souza Jr., lab staff from INDT, for their continuous effort and support with the measurement setup; as well as to Leandro Conceição, and Sergio Abreu, also from INDT, for their kind and valuable collaboration during the measurement campaign.

REFERENCES

[1] P. Mogensen *et al.*, " Centimeter-Wave Concept for 5G Ultra-Dense Small Cells", *IEEE Vehicular Technology Conference (VTC)*, May 2014.

[2] T. S. Rappaport *et al.*, "Millimeter Wave Wireless Communications", 1st Edition, Prentice Hall, 2015.

[3] Mobile and wireless communications Enablers for the Twenty Twenty Information Society (METIS2020), "Deliverable D5.1, Intermediate description of the spectrum needs and usage principles", August, 2013.

[4] J. Maurer *et al.*, "Wideband Wave Propagation Measurements for Local Multipoint Distributions Services (LMDS) at 26 GHz", *IEEE Vehicular Technology Conference (VTC)*, September 2000.

[5] S. Y. Seidel, "Radio Propagation and Planning at 28 GHz for Local Multipoint Distributions Services (LMDS)", *IEEE Antennas and Propagation Society International Symposium*, vol. 2, 1998.

[6] Y. Azar *et al.*, "28 GHz Propagation Measurements for Outdoor Cellular Communications using Steerable Beam Antennas in New York City", *IEEE International Conference on Communications (ICC)*, June 2013.

[7] M. Samimi *et al.*, "28 GHz Angle of Arrival and Angle of Departure Analysis for Outdoor Cellular Communications using Steerable Beam Antennas in New York City", *IEEE Vehicular Technology Conference (VTC)*, June 2013.

[8] S. Sun *et al.*, "Millimeter Wave Multi-beam Antenna Combining for 5G Cellular Link Improvement in New York City", *IEEE International Conference on Communications (ICC)*, June 2014.

[9] G. R. MacCartney Jr. *et al.*, "Exploiting Directionality for Millimeter-Wave Wireless System Improvement", *IEEE International Conference on Communications (ICC)*, June 2015.

[10] T. S. Rappaport *et al.*, "Wideband Millimeter-Wave Propagation Measurements and Channel Models for Future Wireless Communication System Design", *IEEE Transactions on Communications*, vol. 63, no. 9, September 2015.

[11] G. D. Durgin, and T. S. Rappaport, "Theory of Multipath Shape Factors for Small-Scale Fading Wireless Channels", *IEEE Transactions on Antennas and Propagation*, vol. 48, no. 5, May 2000.

[12] K. I. Pedersen *et al.*, "A Stochastic Model of the Temporal and Azimuthal Dispersion Seen at the Base Station in Outdoor Propagation Environments", *IEEE Transactions on Vehicular Technology*, vol. 49, no. 2, March 2000.

[13] Z. Muhi-Eldeen *et al.*, "Performance Analysis of Reflection Paths for Millimeter Wavelength Systems", *IEEE/ACS International Conference on Computer Systems and Applications (AICCSA)*, 2007.

[14] H. Zhao *et al.*, "28 GHz Millimeter Wave Cellular Communication Measurements for Reflection and Penetration Loss in and around Buildings in New York City", *IEEE International Conference on Communications (ICC)*, June 2013.

[15] M. Peter *et al.*, "On Path Loss Measurement and Modeling for Millimeter-wave 5G", *European Conference in Antennas and Propagation (EuCAP)*, June 2015.

[16] I. Rodriguez *et al.*, "Radio Propagation into Modern Buildings: Attenuation Measurements in the Range from 800 MHz to 18 GHz", *IEEE Vehicular Technology Conference (VTC)*, September 2014.

[17] I. Rodriguez *et al.*, "Analysis of 38 GHz mmWave Propagation Characteristics of Urban Scenarios", *European Wireless (EW) Conference*, May 2015.